ASCE

Streamline-Based Method for Reconstruction of Complex Braided River Bathymetry

Ruixun Lai, Ph.D., Aff.M.ASCE[1]; Min Wang[2]; Xiaoli Zhang[3]; Libing Huang, Ph.D.[4]; Fangxiu Zhang[5]; Ming Yang, Ph.D.[6]; and Ming Wang[7]

Abstract: Reconstruction of complex braided river bathymetry is important for supporting hydrodynamic simulation and understanding river morphological processes. To our knowledge, existing methods generate and interpolate channel-fitted coordinate lines using the measured cross-sectional data to reconstruct river bathymetry. Nevertheless, in these methods, the generation of channel-fitted lines obeys the law of splines or a set of equations without considering the laws of river dynamics. Moreover, it is difficult to interpolate bathymetry using the channel-fitted lines when dealing with complex braided rivers. This paper introduced a novel method to fill the gap. Briefly, in the introduced method, an initial bathymetry is interpolated and a velocity field is calculated using a set of simplified two-dimensional (2D) shallow-water equations. Then, streamlines are generated using the velocity field data, and the elevations of the nodes on the streamlines are interpolated using the measured cross-sectional data. Finally, the bathymetry of the domain is interpolated using the streamlines and the measured elevation points or contour lines at the sandbars and floodplains. For demonstration purpose, the introduced method was applied to a 20-km section in the middle reaches of the Yellow River (China) with many branches and sandbars. The reconstructed bathymetry of the domain was investigated in terms of their geometrical shape and hydrodynamic performance (including inundation area and water level). When compared with the measured water level, the hydrodynamic results of the reconstructed bathymetry showed acceptable accuracy. In addition, because the channel-fitted method is widely applied to interpolate the river bathymetry, we compare the channel-fitted method with the introduced method in discussion section. **DOI: 10.1061/(ASCE)HE.1943-5584.0002080.**

Author keywords: River bathymetry; Braided river; Shallow-water equations; Streamline.

Introduction

A shallow-water numerical model is widely applied to simulate river dynamics as a function of inundation area, velocity, and depth. Knowledge about the variables simulated in such models is important to support the modern environmental and engineering challenges, such as water supply and flood risk assessment (e.g., Costabile et al. 2017; Guinot et al. 2017; Pender and Ne'elz 2010), dispersion of pollutants (e.g., Vanzo et al. 2016), disturbance of freshwater habitats (e.g., Choi et al. 2015; He et al. 2009), sedimentation (e.g., Cao et al. 2017), bridge piers (e.g., Larsen et al. 2011), and river morphology (e.g., Karmaker and Dutta 2016). In a numerical model, accurate representation of the river terrain (especially the bathymetry) is critical for deriving these flow features (Javernick et al. 2016).

There are several advanced techniques suitable for acquiring the river bathymetry, which include the multibeam sonar systems (Nittrouer et al. 2008), airborne bathymetric light detection and ranging systems (McKean et al. 2009, 2014), and optical remote sensing imaging methods (Legleiter and Harrison 2019). The multibeam echo sounders or sonar systems acquire the bathymetry via active sensing which provides spatially smooth and high-resolution topographical data (Colbo et al. 2014; Nittrouer et al. 2008). Nevertheless, the application of a sonar system in shallow-water environments is relatively rare because of the difficulty in realizing seamless data between the water body and dry land (Costa et al. 2009). Therefore, the sonar measurement systems are primarily adopted in coastal and seafloor applications (Zhi et al. 2014). The light detection and ranging systems (or remote sensing imaging) involve the detection of visible and near-infrared radiation in the process of mapping the bathymetry in river systems. While the bathymetry could be mapped remotely under conditions of reasonable sediment concentration, previous simulation studies suggested that such applications could be restricted to shallow depths and subjected to a degree of uncertainty (Cao et al. 2019; Legleiter et al. 2011a, b, c). Although these advanced techniques could provide some bathymetric data with high temporal and spatial resolutions,

[1]Senior Engineer, Dept. of Sedimentation Research, Yellow River Institute of Hydraulic Research, Zhengzhou 450003, China (corresponding author). ORCID: https://orcid.org/0000-0001-6128-624X. Email: lairuixun@163.com

[2]Senior Engineer, Dept. of Information Center, Yellow River Institute of Hydraulic Research, Zhengzhou 450003, China. Email: 15491413@qq.com

[3]Senior Engineer, Dept. of Sedimentation Research, Yellow River Institute of Hydraulic Research, Zhengzhou 450003, China. Email: 37668260@qq.com

[4]Senior Engineer, Dept. of Sedimentation Research, Yellow River Institute of Hydraulic Research, Zhengzhou 450003, China. Email: 8839hlb@163.com

[5]Senior Engineer, Dept. of Sedimentation Research, Yellow River Institute of Hydraulic Research, Zhengzhou 450003, China. Email: 253545768@qq.com

[6]Senior Engineer, Dept. of Sedimentation Research, Yellow River Institute of Hydraulic Research, Zhengzhou 450003, China. Email: 86001236@qq.com

[7]Senior Engineer, Dept. of Sedimentation Research, Yellow River Institute of Hydraulic Research, Zhengzhou 450003, China. Email: wangming198261@163.com

Note. This manuscript was submitted on April 14, 2020; approved on December 28, 2020; published online on February 19, 2021. Discussion period open until July 19, 2021; separate discussions must be submitted for individual papers. This paper is part of the ***Journal of Hydrologic Engineering***, © ASCE, ISSN 1084-0699.

they could be quite time-consuming and expensive (Glenn et al. 2016).

In most cases, a set of measured elevation points and cross-sectional data might represent the only means of representing river topography. Such data provide a valuable record of historical river topography, and can be adopted to calibrate parameters such as roughness coefficient in practical applications (Le et al. 2020). The availability of such data has motivated the development of interpolation algorithms for reconstructing river terrains. In general, these algorithms first introduce a curvilinear orthogonal mesh restricted by the water body and thalweg. Then, measured cross-sectional data are imposed on the streamwise lines of the mesh to interpolate the bathymetry of the rivers (Thanh et al. 2020; Caviedes-Voullième et al. 2014; Lai et al. 2018; Merwade 2009; Merwade et al. 2008, 2005).

Most of the interpolation algorithms discussed previously are only applicable to single-channel streams instead of braided rivers. Nonetheless, braided rivers are more common than other river channel patterns, e.g., straight, meandering, and sinuous (Mangelsdorf et al. 1990). Briefly, the morphology of a braided river constitutes a number of alluvial channels divided by islands or sandbars, which might converge and bifurcate repeatedly (Leopold and Wolman 1957). The braiding of rivers is affected by many factors, such as the discharge, size distribution of the bed material, and sediment load (Garde 2006). In a braided river system, these factors interact and vary rapidly both temporally and spatially, causing erosion and deposition in different areas (Wheaton et al. 2009). In this sense, reconstructing a braided river system is more challenging compared to reconstructing other river patterns (Williams et al. 2015).

Some recent studies suggested that the reconstruction of complex river morphologies with islands would require a manual intervention process (Schäppi et al. 2010). To simplify the process, Hilton et al. (2019) introduced a novel and efficient method to generate a coordinate system fitted to the river channel. In Hilton et al. (2019), a dimensionless conformal coordinate system was defined and the bathymetry was interpolated using measured data. Then, the interpolation was projected back to the real-world coordinates. That method was applied to reconstruct the river morphology, and was shown to be capable of handling topographic features, such as island.

While existing interpolation methods can successfully reconstruct river morphologies with islands, very few studies examined their applications for the reconstruction of complex morphology, such as braided rivers. The major disadvantage of the channel-fitted method is the difficulty of mesh generation when the geometry of sandbars are considered as inner boundaries. Moreover, in previous studies, the streamwise lines that are applied for interpolation obey the law of splines or equations rather than the law of river dynamics. The drawbacks of the channel-fitted mesh will be compared with the introduced method in detail in the "Discussion" section.

In this paper, we introduce a novel method for reconstructing the complex morphology of braided rivers. To do so, we first generate an initial bathymetry and calculate a velocity field based on a set of simplified two-dimensional (2D) shallow-water equations. Then, streamlines of a braided river are generated to represent the trajectories of fluid particles. Based on the streamlines, measured cross-sectional data are imposed to interpolate the elevation value of the nodes between the nearest cross sections. Next, we validate the proposed method using the measured data. This is performed by analyzing the geometry of the interpolated cross sections and the performance of the reconstructed topography. For demonstration purposes, we apply the proposed algorithm to reconstruct a 20-km section in the middle of the Yellow River (China), which has many sandbars and branches. We test the performance of the reconstructed river terrain using the 2D shallow-water equations to evaluate the inundation area and water level. Finally, we conclude whether the proposed method can reliably rebuild the bathymetry of a braided river with acceptable accuracy.

Method

General Process of Reconstruction of a Braided River

To illustrate the reconstruction process, a schematic of a braided river is presented in Fig. 1. The available data in the braided river include three cross sections and the location of sandbars. Cross-sections I and II contain two channels divided by sandbars, while Cross-section III has a single channel that is considered as downstream. The challenge is to figure out how to use the available data to interpolate bathymetry between the cross sections. In our proposed method, our main idea is to first interpolate an initial bathymetry to generate streamlines in the x–y plane between the upstream and the downstream. Then, we interpolate the elevation value of the nodes at the streamlines using the cross-sectional data to improve the initial bathymetry.

The first step is to identify the boundary, in an x–y plane, between water bodies and sandbars in the river [Fig. 1(a)], which can be measured directly or extracted from images. To generate the streamlines of the domain, an initial bathymetry and a computational mesh must be prepared. The initial bathymetry is restricted to within the water body and is interpolated linearly based on cross sections from the upstream to the downstream [Fig. 1(b)]. It is ideal to use an unstructured mesh to partition the domain because the geometric shape of the water body is complex and could be complex in a real-world braided river [Fig. 1(c)]. To calculate the velocity field, a set of simplified shallow-water equations discretized using the finite volume method is applied [Fig. 1(d)].

Streamlines are generated based on the velocity data [Fig. 1(e)]. Because the average elevation at the upstream is always higher than the downstream, there must be a slope of the initial bathymetry, which makes the generated streamlines represent the movement of fluid particles in the x-y plane. In the vertical direction, the elevation value of the nodes at the streamlines is interpolated twice using all the measured cross-sectional data to form three-dimensional (3D) streamlines [Fig. 1(f)]. The first is the interpolation of the nodes that intersect with the cross sections, while the second is the interpolation between the cross sections. At this point, the initial bathymetry under water is improved by the measured cross-sectional data.

After the interpolation of streamlines, the data from the streamlines and the elevation data at the sandbars or floodplain are imposed to build the bathymetry of the river. Details about the interpolation of initial bathymetry, generation of streamlines and its interpolation are described subsequently.

Interpolation of Initial Bathymetry

Assuming that the data are given in the form of three cross sections [Fig. 1(a)], Cross-sections I and III would represent the upstream and downstream, respectively (Fig. 2). Owing to the complex shape of the cross sections and limited bathymetric data between them, the creation of the initial bathymetry can be difficult. To address this issue, we generalize the real-world cross sections into a rectangle shape denoted as represented cross sections, which keeps the basic characteristics of the actual cross sections. Then, we use the

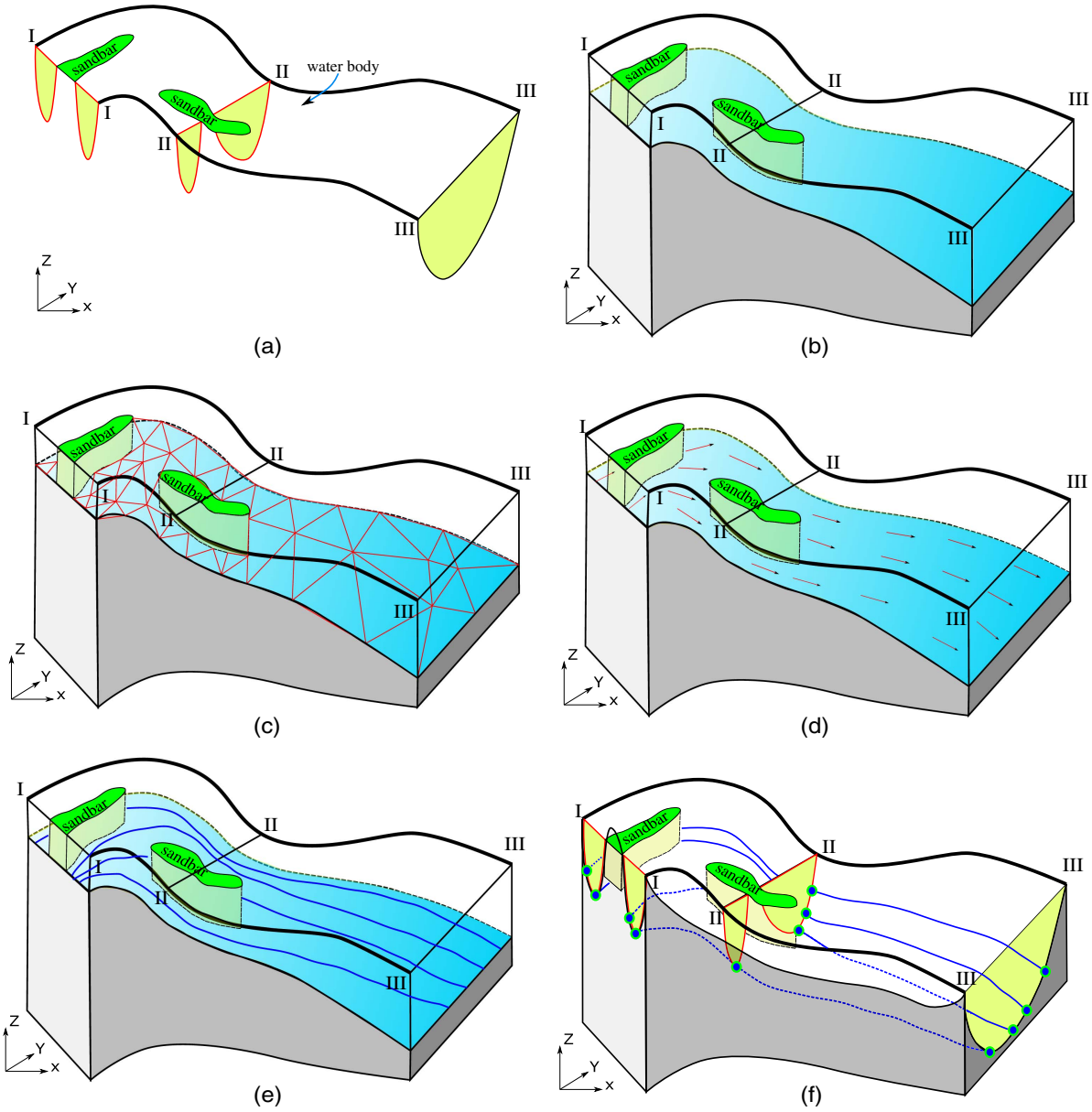

Fig. 1. Schematic of the process adopted for reconstruction of the bathymetry of a braided river: (a) cross sections and water body; (b) initial bathymetry linearly interpolating from upstream to downstream; (c) computational mesh; (d) calculating velocity field using simplified shallow water equations; (e) generating streamlines; and (f) interpolating elevation of streamlines using measured cross sections.

measured data to calculate the bottom elevation of the represented cross sections for the interpolation of the initial bathymetry.

Using the upstream cross sections as an example, the geometric characteristics of the cross sections include the water level and width of each channel, denoted in Fig. 2 as Z and B, respectively. The flow cross-sectional area normal to the direction of the flow is denoted as A. If there are multiple channels, these characteristics are numbered in ascending order for each channel. For the represented cross sections, the water level of the cross section is calculated as the average water level of all-natural channels, while the width and wetted area of the cross section are aggregated for all water bodies. Thus, the characteristics of the cross section can be described mathematically as

$$Z_{us}^{\text{top}} = \frac{1}{n}\sum_{i=1}^{n} Z_i \tag{1}$$

$$B_{us} = \sum_{i=1}^{n} B_i \tag{2}$$

$$A_{us} = \sum_{i=1}^{n} A_i \tag{3}$$

where i = number of a specific channel; and n = total number of channels; Z_{us}^{top} = water level of the represented cross section at the upstream; and B_{us} and A_{us} = total width and area of the water body, respectively.

Mathematically, the represented cross section has the same wetted area as the actual cross section. The wetted area of the represented cross section contains the following relationship:

$$(Z_{us}^{\text{top}} - Z_{us}^{bom}) \times B_{us} = A_{us} \tag{4}$$

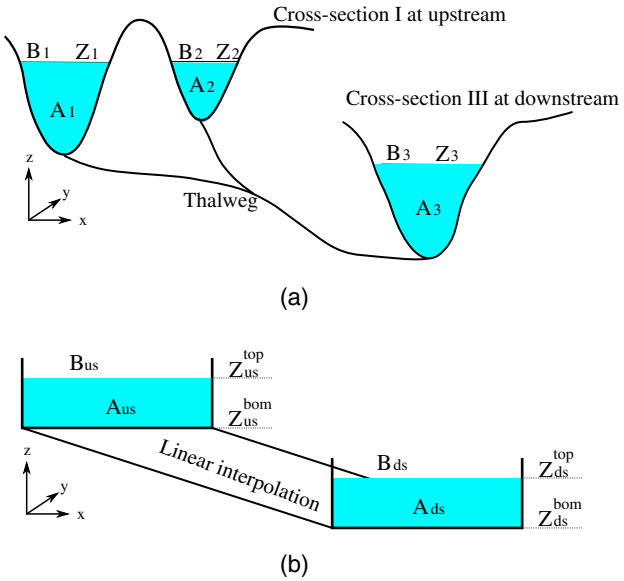

Fig. 2. Linear interpolation of an initial bathymetry: (a) real-world cross sections; and (b) represented cross sections.

where Z_{us}^{bom} is the bottom value of the represented cross section; and $Z_{us}^{top} - Z_{us}^{bom}$ is its depth. Consequently, the bottom of the upstream cross section, Z_{us}^{bom}, is redefined as

$$Z_{us}^{bom} = Z_{us}^{top} - \frac{A_{us}}{B_{us}} \tag{5}$$

Similarly, the bottom value of the represented cross section at the downstream can be calculated as

$$Z_{ds}^{bom} = Z_{ds}^{top} - \frac{A_{ds}}{B_{ds}} \tag{6}$$

where variables A, B, and Z on the right side of Eqs. (5) and (6) can be measured in the field and calculated using Eqs. (1)–(3). When the river flows from the upstream to the downstream, the bottom value at the upstream, Z_{us}^{bom}, is higher than the value at the downstream. The initial bathymetry of the braided river is interpolated linearly using the bottom values at the upstream (Z_{us}^{bom}) and the downstream (Z_{ds}^{bom}). In this step, the domain of the braided river is restricted to within the water edge, i.e., the areas of sandbars and floodplains are excluded.

Calculation of the Velocity Field

To calculate the velocity field of the initial bathymetry [Fig. 1(d)], a set of simplified 2D shallow-water equations is adopted. While the full 2D shallow-water equations are widely applied in computational river dynamics (Katopodes 2018; Chaudhry 2008; Vreugdenhil 1994), simplifications are possible when interpolating streamlines of braided rivers.

The first simplification is to remove the driving forces, such as the Coriolis force, atmospheric pressure gradient, wind stress vector on the water surface, density gradients, and tidal stresses. In the momentum equation, the gravitational force that acts directly on the volumetric mass of the fluid element is considered, but the surface forces (including the pressure distribution and the shear acting on the surface) are removed. The stress on the channel bottom, imposed via friction, is considered and expressed through the Manning equation with dependence on the depth-averaged velocity and roughness.

For these simplifications, a cell-centered finite volume is formulated and the integral form of the unsteady shallow-water equations can be written as (Kuiry et al. 2008)

$$\int_{\Omega} \frac{\partial \mathbf{U}}{\partial t} d\Omega + \int_{\Omega} \nabla \cdot (\mathbf{E}, \mathbf{G}) d\Omega = \int_{\Omega} \mathbf{S} d\Omega \tag{7}$$

in which

$$\mathbf{U} = \begin{pmatrix} H \\ hu \\ hv \end{pmatrix}, \quad \mathbf{E} = \begin{pmatrix} hu \\ hu^2 + \frac{1}{2}gh^2 \\ huv \end{pmatrix},$$

$$\mathbf{G} = \begin{pmatrix} hv \\ hvu \\ hv^2 + \frac{1}{2}gh^2 \end{pmatrix}, \quad \mathbf{S} = \begin{bmatrix} 0 \\ -gh\left(\frac{\partial Z_b}{\partial x} + \tau_{bx}\right) \\ -gh\left(\frac{\partial Z_b}{\partial y} + \tau_{by}\right) \end{bmatrix}$$

where Ω = domain of interest; $\mathbf{E}$ and $\mathbf{G}$ = convective fluxes in the x- and y-directions, respectively; $\mathbf{S}$ = source terms that involve friction and bed slope; H = water surface; h = water depth above the bottom Z_b; u and v = velocity in the streamwise and transverse directions, respectively; g = gravitational force; and τ_{bx} and τ_{by} = frictional bottom stress vectors in the plane direction (Fennema and Chaudhry 1990).

An unstructured triangular mesh (Liseĭkin 2010) is applied to discretize the computational domain, which can fit the irregular shape of a braided river. A cell-centered scheme for which all the state variables are updated at the centroid of each cell is used for defining the control volume (Blazek 2015). Based on the Gauss divergence theorem, Eq. (7) is discretized via transformation from a volume integral to a surface integral. The numerical flux of the convection term across a cell interface is solved using Roe's approximate Riemann scheme (Roe 1997; Glaister 1990). Following Valiani and Begnudelli (2006) and Beffa and Connell (2001), we use numerical treatments to determine the bottom slope source term and the friction slope source term.

Regarding the boundary conditions of the numerical model, an unsteady flow condition starting from zero to peak is given at the upstream, whereas a rating curve is defined at the downstream. The peak flow should be equal to the value at the time when the cross section and water edge was measured. Consequently, the calculated velocity field would maintain the same situation as at the time of measurement.

Generation of Streamlines

The generation of streamlines [Fig. 1(e)] depends on the velocity field. When the solution of the velocity field stabilizes, the velocity field provides a snapshot of the direction of movement of fluid particles in a river. These particles form trajectories that transport mass, interact with bed material, and shape the river bathymetry. In such situation, these trajectories become streamlines represented by a family of curves instantaneously tangential to the velocity vector of the flow that show the direction of travel of fluid elements at any point in time. For 2D flow in the x–y plane [Fig. 3(a)], the slope of the streamline (dy/dx) must equate the tangent of the local instantaneous velocity vector (Çengel and Cimbala 2018; Granger 1995). The numerical solution of streamlines depends on the

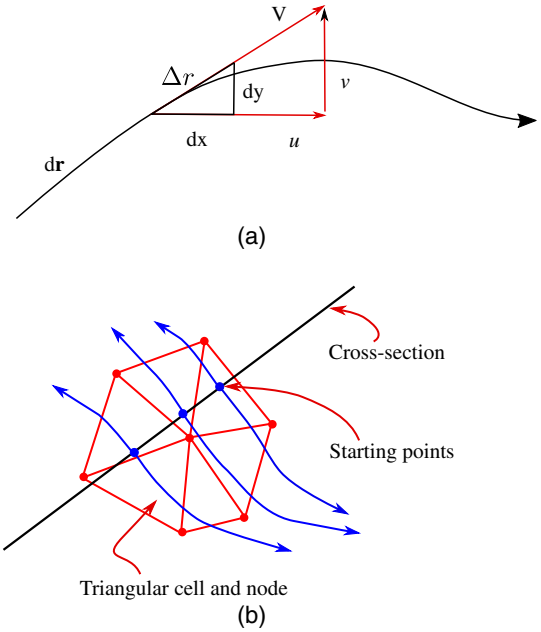

Fig. 3. Numerical solution of a streamline and the seeding of starting points: (a) numerical solution of streamline; and (b) starting points and its interpolation based on velocity field.

streamline functions (Kundu et al. 2016; Dalena et al. 2012), and can be solved numerically using the Runge–Kutta method (Qin et al. 2019; Ueng et al. 1995).

Another issue is related to the starting points or seeding points of the generated streamline. There are several ways of seeding streamlines (Lefer and Grave 2013). Nevertheless, there is still no systematic way of implementing a seeding strategy (Ye et al. 2005). In this study, because the bathymetry should be generated using the measured cross-sectional data, the starting points would start from the locations of the cross sections displayed in Fig. 3(b). Following that, the location of a streamline is calculated in the forward or backward direction.

Interpolating Bathymetry Using Streamlines and Other Data

Following Lai et al. (2018) and Caviedes-Voullième et al. (2014), we interpolate the elevation of nodes along the streamlines [Fig. 1(f)]. Specifically, the elevation of the nodes intersecting with a cross section is first interpolated based on the cross section itself. Then, the nodes on a streamline are interpolated linearly based on two adjacent cross sections to produce 3D nodes (Fig. 4). Next, the bathymetry of the entire river is interpolated using data from the 3D nodes of the streamlines, elevation points at the sandbars, and contour lines of the surrounding floodplains in order to conform to a digital elevation model in a form of triangular irregular network (El-Sheimy et al. 2005).

Application

Study Area and Data

We apply the proposed method to the Longmen–Tongguan section (length: 132.5 km) in the middle reaches of the Yellow River, China (Fig. 5). In the selected reach, when the river flow exits the Yumenkou Gorge, the river channel widens abruptly into a wide braided plain with average width of 8.5 km (Li 2009). The banks on either side are 10–200 m higher than the riverbed. The elevation difference from Longmen to Tongguan is approximately 55 m, and the longitudinal gradient of the river varies gradually from 3.0‰ to 6.0‰ (Wang et al. 2020). In the selected section, the river course is unstable with frequent rapids, causing the growth and migration of sandbars and the formation of many branches.

The river contains some hyperconcentrated sediment. In the period 1919–2000, the annual runoff recorded at the Longmen station was 29.7 billion m^3, and the annual sediment yield was approximately 0.897 billion tons. However, until 2010, the annual runoff and annual sediment yield dramatically declined to 20.5 billion m^3 and 0.0776 billion tons, respectively (Zheng et al. 2015). In 2010, a bridge was built across the upper section of the study area, and a numerical hydrodynamic model was applied to calculate the inundation area. Therefore, the reconstruction of the river bathymetry was performed before that calculation. The area

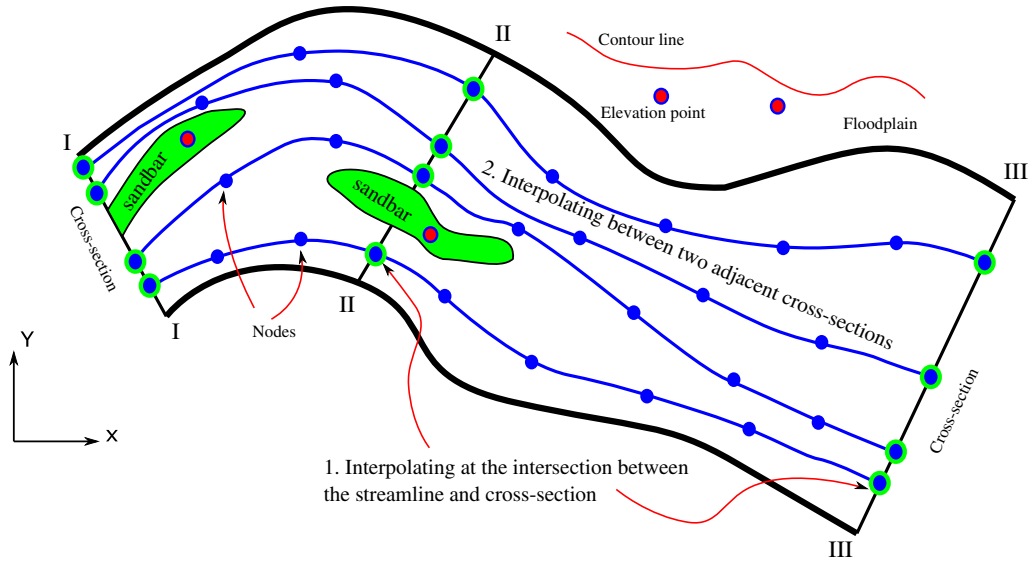

Fig. 4. Interpolation of bathymetry using streamlines and other data.

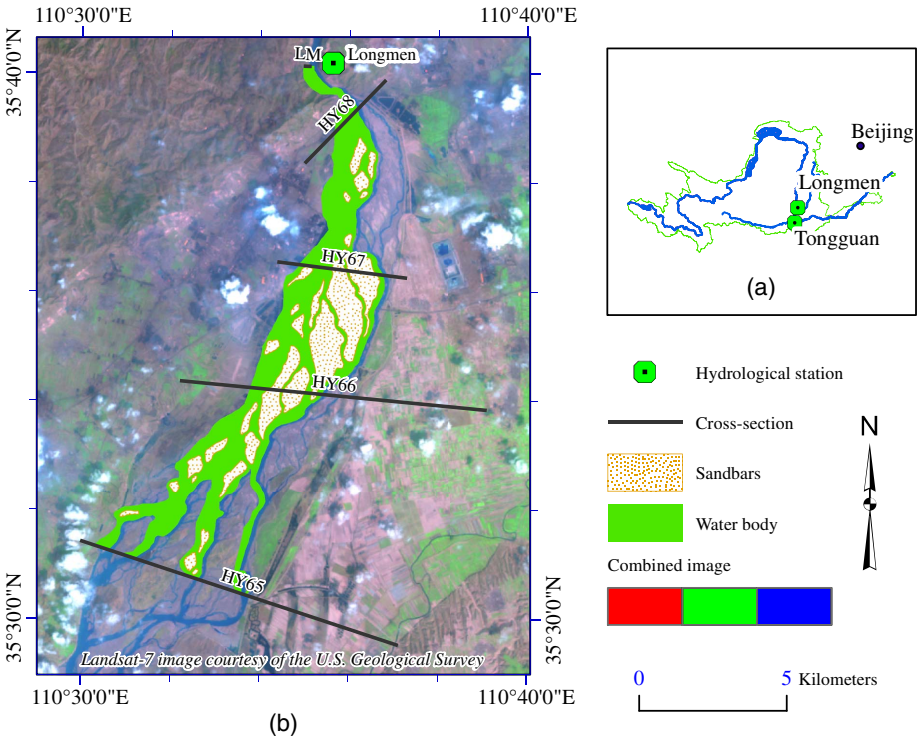

Fig. 5. Application area: (a) Yellow River basin; and (b) application area (Landsat-7 image courtesy of the US Geological Survey).

selected for the reconstruction (with 27 sandbars) was from Cross-section LM to HY65, a total of 20 km (Fig. 5).

In April 2010, five cross sections were measured for which the average distance between two adjacent cross sections was 5 km. The locations of the five cross sections have been determined since 1960 because of the construction of the Sanmenxia Reservoir. The cross-sectional data were measured by following the Chinese technical standard for general geodesic survey in hydrology. The whole cross section (including the wet and dry topography) was measured. The positions of the survey points were recorded using GPS, while the depth was measured using echo sounder or sounding rod. The cross-sectional spacing was determined from the width of the water surface.

Reconstruction of the River Bathymetry

According to the process introduced in the method section, the first step is to identify the boundary of water body in x-y plane. In this work, we use the Landsat 7 imagery (acquired on April 15, 2010) to identify the water edge boundary. Briefly, the Enhanced Thematic Mapper Plus sensor onboard Landsat 7 is an eight-band multispectral scanning radiometer capable of providing 30-m-resolution imaging information (Chastain et al. 2019). It detects spectrally filtered radiation in the visible, near-infrared, midinfrared, and far-infrared wavebands. For sharp definition of the edge between a water body and sandbar, information from the near-infrared, midinfrared, and red regions of the spectrum was combined (Campbell and Wynne 2011), as shown in Fig. 5(b). Using the displayed image as a base map, the results of the water body detection show that the main channel from Cross-section LM to HY67 is near to the west bank of the river [Fig. 6(a)]. From Cross-section HY67 to HY65, the river is divided into several branches around a number of sandbars. At the downstream of the domain, four branches flow into the lower river reach.

The second step in the process is to interpolate the initial bathymetry using Cross-sections of LM and HY65. On April 15, 2010, the water level of the Cross-section LM was approximately 384 m, while its average bed elevation was 380.8 m [calculated using Eq. (5)]. At Cross-section HY65, there were four branches for which the average bed elevation was calculated as 369.7 m. Consequently, the initial bathymetry is considered to decrease linearly from the upstream to the downstream, and the slope is assumed as 5.5‰ along the longitudinal profile [Fig. 6(b)].

The next step is to calculate the velocity field and generate the streamlines within the domain of water body. Unstructured mesh with over 120,000 cells is adopted to partition the domain [Fig. 6(c)], and Eq. (7) is applied to reproduce the velocity field. On April 15, the average daily discharge at Cross-section LM was 855 m^3/s, and the Manning roughness coefficients within the main channel was calibrated to be 0.020 $s \cdot m^{-1/3}$. With the velocity field information, 42 streamlines are generated [Fig. 6(d)]. Despite the presence of branches, the detailed section near Cross-section HY67 shows that the generated streamlines flowed through the river and filled the water body. Although there were sandbars in the domain, the generated streamlines passing from the upstream to the downstream can represent the trajectories of the fluid particles that shaped the riverbed.

To investigate the performance of the introduced method, two cases of interpolation strategy are applied. In Case 1, all the measured cross sections are used to interpolate the streamlines [Fig. 6(e)]. While Case 2 shares the same streamlines as Case 1, the streamlines are interpolated using the selected cross sections at the upstream and the downstream [Fig. 6(f)]. In other words, in Case 2, the Cross-sections HY68, HY67, and HY66 are excluded in the process of channel interpolation. Comparing to the result of the initial bathymetry [Fig. 6(b)], there are significant changes within the water edge. Principally, the bathymetry of the main channel no longer decreases linearly from the upstream to the

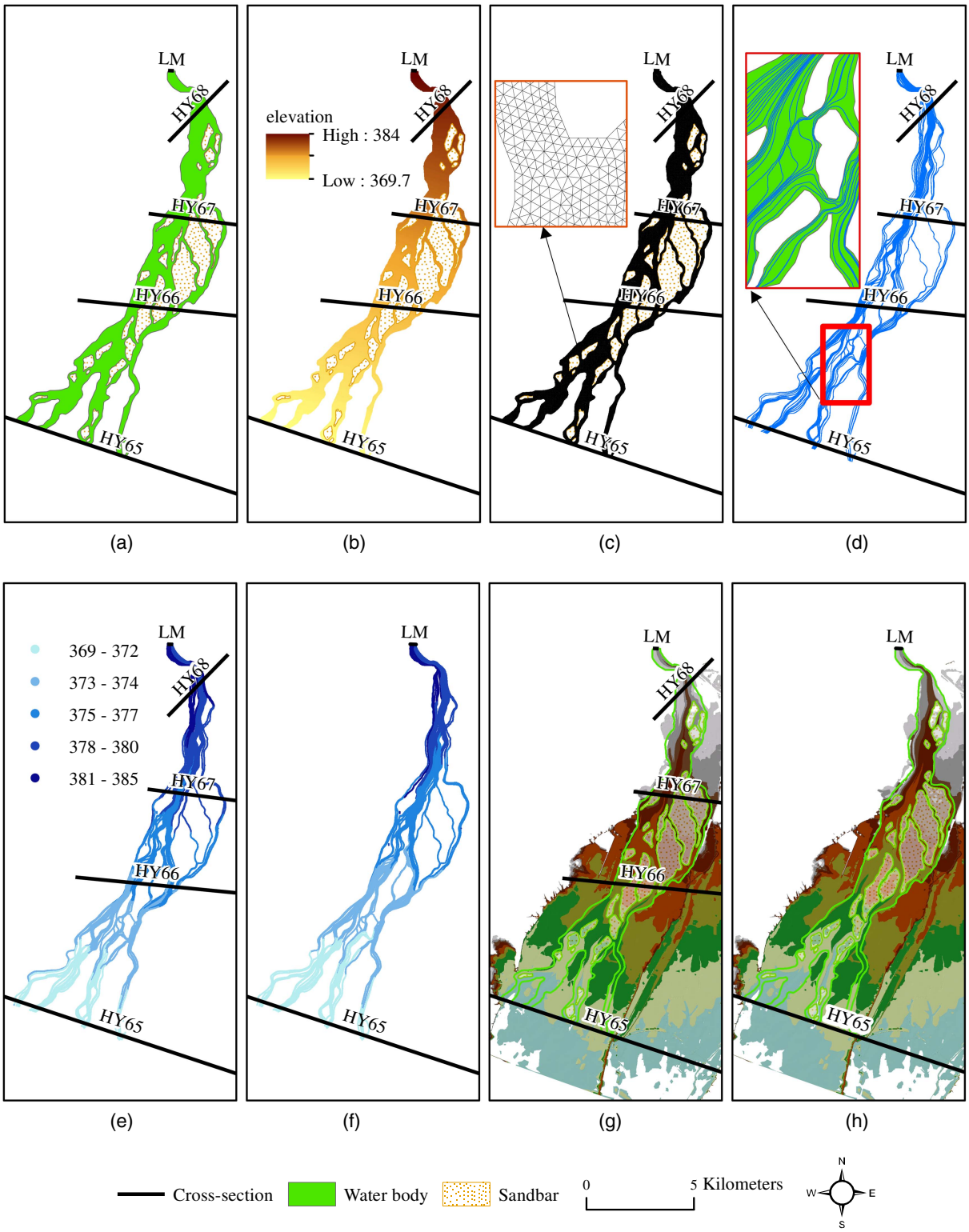

Fig. 6. Process adopted to reconstruct the river terrain model: (a) water body; (b) initial bathymetry; (c) mesh; (d) streamlines; (e) 3D streamlines using all cross sections; (f) 3D streamlines using two cross sections; (g) result of Case 1; and (h) result of Case 2.

downstream, but the main channels are deeper, as shown in Cross-sections HY68 and HY67. This confirms that the interpolation algorithm is useful between the cross sections.

As soon as the streamlines are interpolated based on the cross-sectional data, the streamlines are then interpolated by considering the contour lines and elevation points around the channels to build the river terrain of the entire domain. Case 1 and Case 2 share the same elevation data around the channels, and the results of the reconstructed river terrain model for the two cases are displayed in Figs. 6(g and h), respectively.

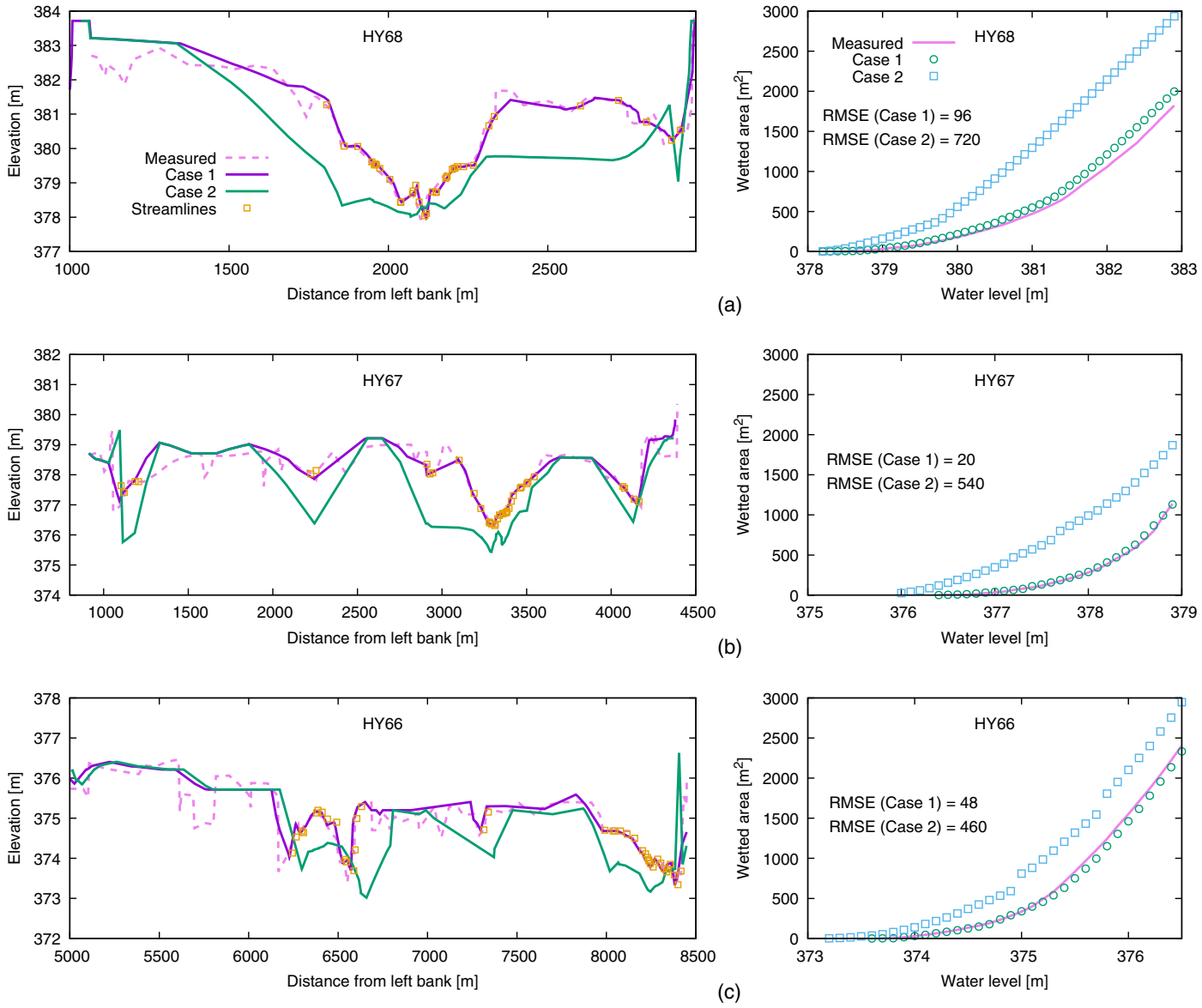

Fig. 7. Comparison of the reconstructed river terrain with the measured cross sections.

Performance of the Reconstructed River Terrain Model

We examine the performance of the reconstructed river terrain model from two perspectives: the geometric quality, in which the geometric shape and wetted area of the cross section are investigated; and the hydrodynamic results of the terrain model, in which the inundation area and water level are evaluated.

Geometry of the Reconstructed Cross Sections

The geometrical characteristics represent the shape of the reconstructed cross sections, whereas the wetted cross-sectional area related to variation in the water level provides an accurate assessment of flow capacity. In Fig. 7, the measured and reconstructed depth profiles and wetted areas for the Cross-sections HY68, HY67, and HY66 are compared after the exclusion of points on the floodplain. In Case 1, Fig. 7 indicates the location of the streamlines that intersect with the cross sections. Overall, the location of the streamlines coincides with the measured cross sections very well.

For Cross-section HY68, a single channel is observed when compared with the measured water level. The reconstructed cross section of Case 1 is accurate with an average root-mean square error (RMSE) value of 96 m^2; whereas that of Case 2 is less accurate with an average RMSE value of 720 m^2, and its cross-sectional flow capacity is overestimated. The wetted areas of these cases indicate the overestimation of the flow capacity of Case 2 compared to Case 1.

Cross-section HY67 contains four channels divided by three sandbars. It is obvious that the elevation of the sandbars can be controlled by the measured elevation points. The performance of the reconstructed bathymetry is similar to that of Cross-section HY68, i.e., the results of Case 1 provide a better shape than those of Case 2.

At the Cross-section HY66, the overall RMSE value of Case 1 (48 m^2) is acceptable. However, the shape derived from the results of Case 2 can change abruptly, especially at the boundary between the water body and the sandbars.

The failure of the results of Case 2 can be investigated by comparing with the thalweg profile (Fig. 8). Although the average longitudinal gradient is 5.5‰, the measured profile does not drop linearly from the upstream to the downstream. Conversely, it

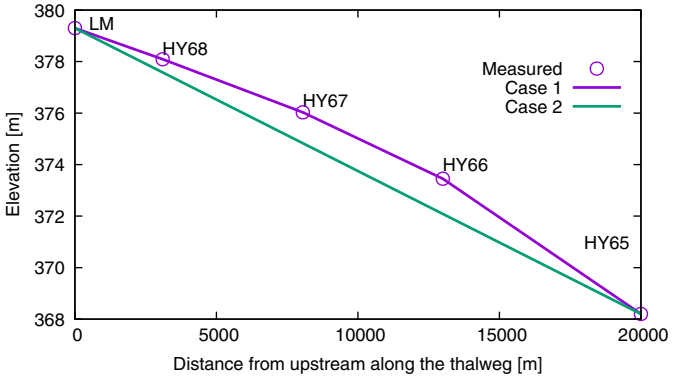

Fig. 8. Reconstructed thalweg line and measured points.

changes in relation to the geometrical profile along the river. Specifically, the slope of the river profile from the Cross-sections HY68 to HY66 (4.4‰) is milder than the average value of the entire river; but it increases sharply from the Cross-sections HY66 to HY65 (7.0‰). The streamlines of Case 2 were interpolated using selected data from the Cross-sections LM and HY65, thus it is difficult to control the geometrical shape. As a result, we get the overestimated cross-sectional flow capacity.

Hydrodynamic Performance

The reconstructed river terrain model is used to simulate the inundation area of April 15, 2010 in order to investigate the performance of the reproduced bathymetry. For this purpose, we apply the 2D shallow-water equations again. The key difference in this hydrodynamic simulation is the simulation domain, which is much larger than that in the generation of streamlines, and covers the water body and floodplain areas.

We perform hydrodynamic simulation on the two cases of the reconstructed river terrain model. We note that both cases share the same computational domain of approximately 72 km^2 [Fig. 9(a)]. To minimize mesh-related errors, we partition the domain into a very fine computational mesh with over than 190,000 unstructured cells. An unsteady flow, starting from 0 and reach to 855 m^3/s after 5 h, is imposed at the upstream (Fig. 10). When the hydrodynamic simulation stabilizes at 855 m^3/s, we get the solution which represents the situation of the acquired water edge data.

The water depth results derived from the two cases are shown in Fig. 9. Overall, the simulated inundations in the two cases are consistent with the extent of the water body extracted from the imagery. However, the sandbars and floodplains remain dry because of their high elevations [Figs. 9(b and c)]. The overestimation of the reconstructed wetted area of Case 2 (relative to the measured value) indicates that the inundation area of Case 2 is smaller than that of Case 1 (Table 1). Specifically, inundation is absent in the easternmost side of the channel in Case 2, as highlighted by the rectangle in Figs. 9(b and c). This is partly because of the shallow depth of this channel (i.e., <0.2 m; as simulated in Case 1), and partly because of overestimated depths of other channels in Case 2. Consequently, the water flows in other channels, which cause the failure of the inundation area in Case 2.

In terms of the simulated water level, Case 1 performs better than Case 2. The simulated water level of Case 2 is lower than that of Case 1, and it deviates quite significantly from the measured data (Table 2). The error in Case 1 is limited to within 0.05 m, whereas the error in Case 2 is greater than that of the measured data.

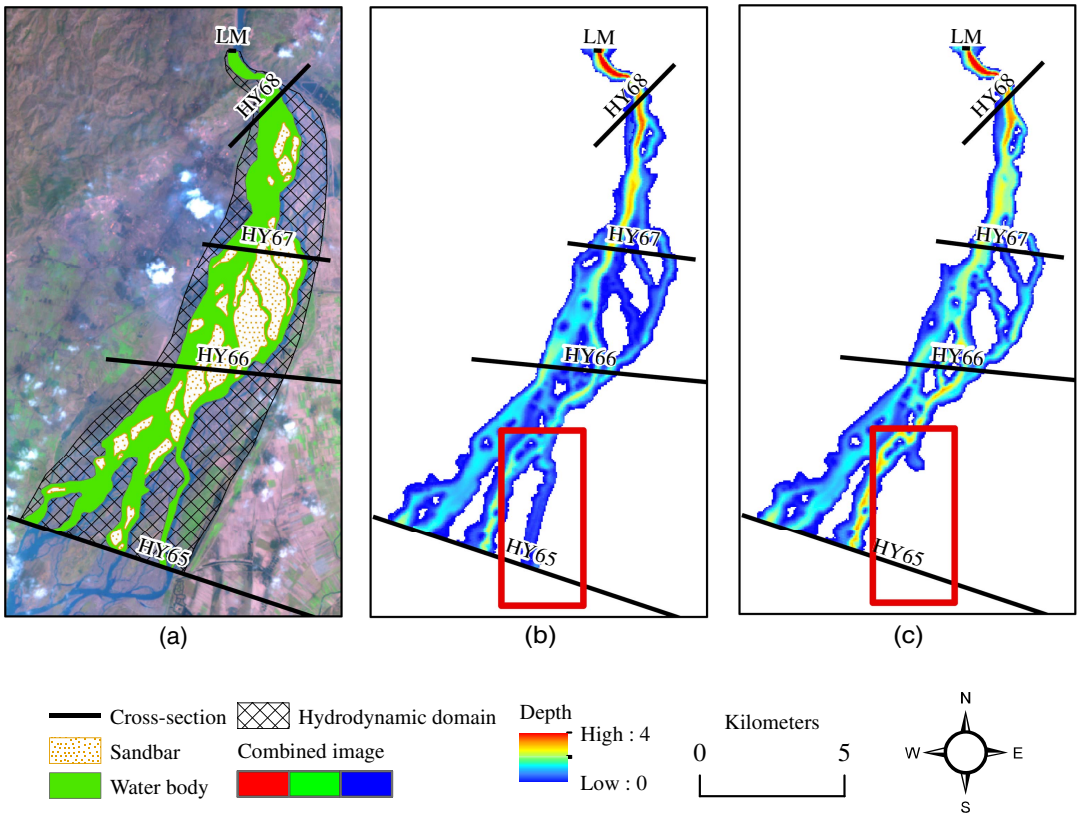

Fig. 9. Results of simulated inundation area and depth: (a) hydrodynamic domain (Landsat-7 image courtesy of the US Geological Survey); (b) depth of Case 1; and (c) depth of Case 2.

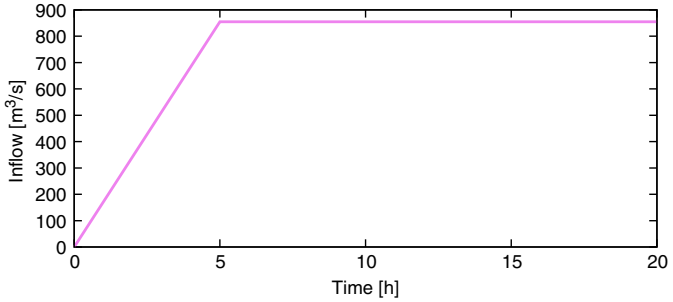

Fig. 10. Inflow discharge.

Table 1. Inundation area of the two cases

Case	Inflow (m^3/s)	Inundation area (km^2)
Case 1	855	37.46
Case 2	855	35.95

Table 2. Comparison of simulated and measured water levels (m)

No. of cross section	Measured	Simulated from Case 1	Simulated from Case 2	Error of Case 1	Error of Case 2
HY68	381.69	381.64	380.15	0.05	1.54
HY67	378.55	378.50	377.26	0.05	1.29
HY66	375.10	375.12	374.52	−0.02	0.58

It indicates that if additional cross sections were applied, the terrain model would be more accurate.

By comparing the geometric and hydrodynamic performances of the two cases of river terrain model, we can see that, although the average distance of the two adjacent cross sections is 5 km, both the geometric shape and hydrodynamic results in Case 1 are quite accurate. Specifically, despite the shallow depth (<0.2 m) in one of the branches, the simulated inundation remains reliable.

Discussion

Because the channel-fitted method is widely applied to interpolate the river bathymetry (e.g., Thanh et al. 2020; Caviedes-Voullième et al. 2014; Merwade et al. 2008, 2005), we discussed the usability of the channel-fitted method to interpolate the bathymetry of braided rivers and compared with the method introduced in this paper.

In general, the channel-fitted mesh uses the orthogonal curvilinear coordinates. The generation of the mesh is numerically solved using spline lines (de Boor 2001) or elliptic equations (Thompson et al. 1985).

Fig. 11 compares the two methods for the interpolation of the bathymetry. Figs. 11(a–d) illustrate the process of mesh-based method, while Figs. 11(f and g) are relative to the streamline-based method. If the braided river of the study area is considered as a single channel, a channel-fitted mesh can be easily generated [Fig. 11(b)]. For the channel-fitted method, the streamwise lines represent the flow particles and are used to interpolate the bathymetry along them. Hence, lines in the transverse direction should be removed [Fig. 11(c)]. If the sandbars are not considered in the domain, the channel-fitted method should be able to properly interpolate the river bathymetry.

However, the fact that many channels are divided by sandbars increases the complexity of interpolation. To interpolate the bathymetry, we must generate a mesh in which each channel [denoted by C1 or C2 in Fig. 11(d)] is generated into a channel-fitted mesh and combined as a whole mesh. Nevertheless, this task can become challenging because the geometric shape of the sandbars is complicated. It must decompose the domain into blocks with simpler topologies and generate structured grids inside each block in turn, a method called the multiblock approach (Cebeci et al. 2005). Furthermore, it is difficult to determine the direction of streamwise line (e.g., left or right as indicated by arrows) from upstream between the two nearest sandbars (S1 and S2) in Fig. 11(d). Thus, some uncertainty exists in generating a channel-fitted mesh with many sandbars.

Until recently, we have not seen any suitable automatic tools for generating channel-fitted mesh that considers the sandbars as inner boundaries. As a result, the generation of channel-fitted mesh for braided rivers is difficult. This is why many previous studies focused on the channel-fitted method for single channel or limited sandbars.

Moreover, the channel-fitted mesh is originally designed for the partition of computational domain and its streamwise lines have no physical basis to represent the trajectory of flow particles that shape the river bed.

Additionally, one may confuse the channel-fitted mesh for interpolation purpose with the channel-fitted mesh for hydrodynamic simulation purpose. For the hydrodynamic purpose, if sandbars are excluded from the domain, the channel-fitted mesh considers the sandbars as inner solid boundaries in which water cannot flow. As shown in Fig. 11(e), the cells at the area of sandbars can be deleted. While this type of channel-fitted mesh can be applied for hydrodynamic simulation, the mesh cannot be used to interpolate the bathymetry because some of its streamwise lines are disconnected between the cross sections [e.g., denoted by bold lines in Fig. 11(e)].

By contrast, the introduced method (streamline-based method) in which streamlines are generated from the results of 2D shallow-water equations can overcome these difficulties. First, unstructured mesh can be used to provide a good representation of complex geometric boundaries of sandbars [Fig. 11(f)]. Second, the generated streamlines [Fig. 11(g)] can represent the trajectory of fluid particles because they are calculated based on velocity field instead of mathematic equations or spline functions. Moreover, if there are additional measured elevations, one can add a seeding point at this point to generate a streamline and improve the accuracy of the bathymetry.

The limitation of the introduced method is related to the characteristics of the flow, which affects the performance of the generated streamlines. For a low Reynolds number flow, viscous effects dominate the resistance to the flow and lead to steady or uniform flow in the streamwise direction. As a result, the generated streamlines are smooth, even behind the sandbars. However, for a high Reynolds number flow, inertia plays a main role in the resistance to the flow, and large eddies are formed behind the sandbars due to the separation of streamlines. The generated streamlines behind the sandbars would be discontinuous, and therefore increase the uncertainty when interpolating bathymetry using adjacent cross sections. In this sense, the introduced method is more suitable for a low Reynolds number flow. For a high Reynolds number flow, more measured data should be added to the interpolated bathymetry behind the sandbars in order to improve the accuracy.

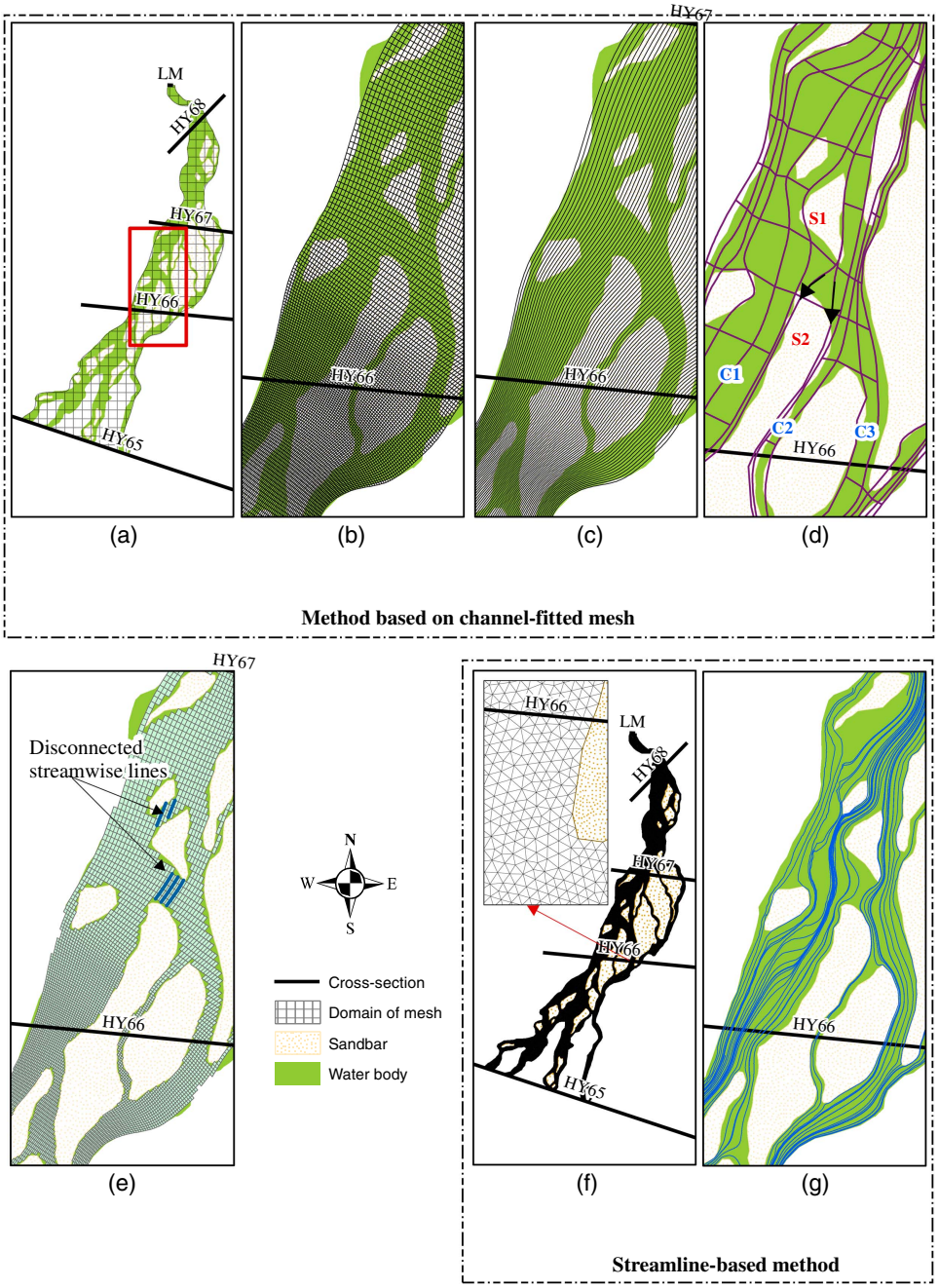

Fig. 11. Comparison of channel-fitted and streamline method to interpolate river bathymetry: (a) domain of channel-fitted mesh; (b) result of channel-fitted mesh; (c) streamwise lines of channel-fitted mesh; (d) streamwise lines considering all the sandbars; (e) channel-fitted mesh for hydrodynamic purpose; (f) triangular mesh of the domain; and (g) streamlines generated based on velocity field.

Conclusions

Reconstruction of the bathymetry of braided rivers is essential to support numerical models related to flood risk management and hydrologic engineering challenges. In this paper, we presented a novel approach for the reconstruction of complex braided rivers, which is based on streamlines generated using simplified 2D shallow-water equations and interpolation from the measured cross-sectional data. Although the topological features of real-world braided river can be complex, the generated streamlines can sufficiently represent the movement of fluid particles. The introduced method was applied to reconstruct the bathymetry in a 20-km section of the middle reaches of the Yellow River (China) with many branches and sandbars. Two cases (using different spacing of cross-sectional data) were applied to compare their derived geometrical shapes and wetted areas. The results indicated that the terrain model would be more accurate when extra cross-sectional data were included. To analyze the hydrodynamic performance of the terrain model in terms of inundation extent and water level, an inflow of 855 m^3/s was imposed in the two cases. Despite the shallow depth (<0.2 m) in one of the branches, the simulation of inundation in Case 1 was a success and better than Case 2. When compared with the measured water level, the simulated value in Case 1 was reasonably accurate (despite the sparsity of available data).

Future studies should focus on situations related to complex morphology, e.g., a braided river with higher braiding intensities. Moreover, further investigations could also acquire independent topographic check data (i.e., away from cross sections) to further assess the accuracy of the reconstructed bathymetry.

Data Availability Statement

Some data regarding water edge and velocity field are available at https://github.com/lairuixun/generating_streamlines. A Fortran code, which generates streamlines based on velocity field, streamline function, and numerically solved by Runge–Kutta method, was made available. The nodes of streamlines were transformed into shapefile data format for interpolation.

Acknowledgments

This work was partially funded and supported by the National Natural Science Foundation of China (Grant Nos. 51809108 and 51679102) and Special Foundation for Public-interest Institutes of China (HKY-JBYW-2020-01).

References

Beffa, C., and R. J. Connell. 2001. "Two-dimensional flood plain flow. I: Model description." *J. Hydrol. Eng.* 6 (5): 397–405. https://doi.org/10.1061/(ASCE)1084-0699(2001)6:5(397).

Blazek, J. 2015. *Computational fluid dynamics: Principles and applications*. Oxford, UK: Butterworth-Heinemann.

Campbell, J. B., and R. H. Wynne. 2011. *Introduction to remote sensing*. New York: Guilford Press.

Cao, B., Y. Fang, Z. Jiang, L. Gao, and H. Hu. 2019. "Shallow water bathymetry from WorldView-2 stereo imagery using two-media photogrammetry." *Eur. J. Remote Sens.* 52 (1): 506–521. https://doi.org/10.1080/22797254.2019.1658542.

Cao, Z., C. Xia, G. Pender, and Q. Liu. 2017. "Shallow water hydro-sediment-morphodynamic equations for fluvial processes." *J. Hydraul. Eng.* 143 (5): 02517001. https://doi.org/10.1061/(ASCE)HY.1943-7900.0001281.

Caviedes-Voullième, D., M. Morales-Hernández, I. López-Marijuan, and P. García-Navarro. 2014. "Reconstruction of 2D river beds by appropriate interpolation of 1D cross-sectional information for flood simulation." *Environ. Modell. Software* 61 (Nov): 206–228. https://doi.org/10.1016/j.envsoft.2014.07.016.

Cebeci, T., J. P. Shao, F. Kafyeke, and E. Laurendeau. 2005. *Computational fluid dynamics for engineers: From panel to Navier-Stokes methods with computer programs*. New York: Springer.

Çengel, Y. A., and J. M. Cimbala. 2018. *Fluid mechanics: Fundamentals and applications*. New York: McGraw-Hill.

Chastain, R., I. Housman, J. Goldstein, M. Finco, and K. Tenneson. 2019. "Empirical cross sensor comparison of Sentinel-2A and 2B MSI, Landsat-8 OLI, and Landsat-7 ETM+ top of atmosphere spectral characteristics over the conterminous United States." *Remote Sens. Environ.* 221 (Feb): 274–285. https://doi.org/10.1016/j.rse.2018.11.012.

Chaudhry, M. H. 2008. *Open-channel flow*. New York: Springer.

Choi, S.-U., S. Jung, and S. K. Kim. 2015. "A quasi-2D and quasi-steady hydraulic model for physical habitat simulations: Physical habitat modeling using quasi-2D hydraulic computations." *Ecohydrology* 8 (2): 263–272. https://doi.org/10.1002/eco.1504.

Colbo, K., T. Ross, C. Brown, and T. Weber. 2014. "A review of oceanographic applications of water column data from multibeam echosounders." *Estuarine Coastal Shelf Sci.* 145 (May): 41–56. https://doi.org/10.1016/j.ecss.2014.04.002.

Costa, B. M., T. A. Battista, and S. J. Pittman. 2009. "Comparative evaluation of airborne LiDAR and ship-based multibeam SoNAR bathymetry and intensity for mapping coral reef ecosystems." *Remote Sens. Environ.* 113 (5): 1082–1100. https://doi.org/10.1016/j.rse.2009.01.015.

Costabile, P., C. Costanzo, and F. Macchione. 2017. "Performances and limitations of the diffusive approximation of the 2D shallow water equations for flood simulation in urban and rural areas." *Appl. Numer. Math.* 116 (Jun): 141–156. https://doi.org/10.1016/j.apnum.2016.07.003.

Dalena, S., P. Chuychai, R. L. Mace, A. Greco, G. Qin, and W. H. Matthaeus. 2012. "Streamline generation code for particle dynamics description in numerical models of turbulence." *Comput. Phys. Commun.* 183 (9): 1974–1985. https://doi.org/10.1016/j.cpc.2012.04.022.

de Boor, C. 2001. "A practical guide to splines." In *Applied mathematical sciences*, edited by J. E. Marsden and L. Sirovich, 27. New York: Springer.

El-Sheimy, N., C. Valeo, and A. Habib. 2005. *Digital terrain modeling: Acquisition, manipulation, and applications*. Boston: Artech House Remote Sensing Library, Artech House.

Fennema, R. J., and M. H. Chaudhry. 1990. "Explicit methods for 2D transient free surface flows." *J. Hydraul. Eng.* 116 (8): 1013–1034. https://doi.org/10.1061/(ASCE)0733-9429(1990)116:8(1013).

Garde, R. J. 2006. *River morphology*. New Delhi, India: New Age International.

Glaister, P. 1990. "Approximate Riemann solutions of the two-dimensional shallow-water equations." *J. Eng. Math.* 24 (1): 45–53. https://doi.org/10.1007/BF00128845.

Glenn, J., D. Tonina, M. D. Morehead, F. Fiedler, and R. Benjankar. 2016. "Effect of transect location, transect spacing and interpolation methods on river bathymetry accuracy: River bathymetry." *Earth Surf. Processes Landforms* 41 (9): 1185–1198. https://doi.org/10.1002/esp.3891.

Granger, R. A. 1995. "Fluid mechanics." In *Dover classics of science and mathematics*. New York: Dover Publications.

Guinot, V., B. F. Sanders, and J. E. Schubert. 2017. "Dual integral porosity shallow water model for urban flood modelling." *Adv. Water Resour.* 103 (May): 16–31. https://doi.org/10.1016/j.advwatres.2017.02.009.

He, Z., W. Wu, and F. Douglas Shields. 2009. "Numerical analysis of effects of large wood structures on channel morphology and fish habitat suitability in a southern US sandy creek." *Ecohydrology* 2 (3): 370–380. https://doi.org/10.1002/eco.60.

Hilton, J. E., S. Grimaldi, R. C. Z. Cohen, N. Garg, Y. Li, S. Marvanek, V. R. N. Pauwels, and J. P. Walker. 2019. "River reconstruction using a conformal mapping method." *Environ. Modell. Software* 119 (Sep): 197–213. https://doi.org/10.1016/j.envsoft.2019.06.006.

Javernick, L., D. M. Hicks, R. Measures, B. Caruso, and J. Brasington. 2016. "Numerical modelling of braided rivers with structure-from-motion-derived terrain models: Modelling braided rivers." *River Res. Appl.* 32 (5): 1071–1081. https://doi.org/10.1002/rra.2918.

Karmaker, T., and S. Dutta. 2016. "Prediction of short-term morphological change in large braided river using 2D numerical model." *J. Hydraul. Eng.* 142 (10): 04016039. https://doi.org/10.1061/(ASCE)HY.1943-7900.0001167.

Katopodes, N. D. 2018. "Shallow-water dynamics." In *Free-surface flow*. Oxford, UK: Butterworth-Heinemann.

Kuiry, S. N., K. Pramanik, and D. Sen. 2008. "Finite volume model for shallow water equations with improved treatment of source terms." *J. Hydraul. Eng.* 134 (2): 231–242. https://doi.org/10.1061/(ASCE)0733-9429(2008)134:2(231).

Kundu, P. K., I. M. Cohen, D. R. Dowling, and G. Tryggvason. 2016. *Fluid mechanics*. Boston: Elsevier.

Lai, R., M. Wang, M. Yang, and C. Zhang. 2018. "Method based on the Laplace equations to reconstruct the river terrain for two-dimensional hydrodynamic numerical modeling." *Comput. Geosci.* 111 (Feb): 26–38. https://doi.org/10.1016/j.cageo.2017.10.006.

Larsen, R. J., F. C. K. Ting, and A. L. Jones. 2011. "Flow velocity and pier scour prediction in a compound channel: Big Sioux river bridge at Flandreau, South Dakota." *J. Hydraul. Eng.* 137 (5): 595–605. https://doi.org/10.1061/(ASCE)HY.1943-7900.0000334.

Le, T. B., A. Crosato, and A. M. Arboleda. 2020. "Revisiting waal river training by historical reconstruction." *J. Hydraul. Eng.* 146 (5): 05020002. https://doi.org/10.1061/(ASCE)HY.1943-7900.0001688.

Lefer, W., and M. Grave. 2013. *Visualization in scientific computing '97: Proceedings of the Eurographics Workshop in Boulogne-sur-Mer, France, April 28-30, 1997*. New York: Springer.

Legleiter, C. J., and L. R. Harrison. 2019. "Remote sensing of river bathymetry: Evaluating a range of sensors, platforms, and algorithms on the Upper Sacramento river, California, USA." *Water Resour. Res.* 55 (3): 2142–2169. https://doi.org/10.1029/2018WR023586.

Legleiter, C. J., P. J. Kinzel, and B. T. Overstreet. 2011a. "Evaluating the potential for remote bathymetric mapping of a turbid, sand-bed river. 1: Field spectroscopy and radiative transfer modeling." *Water Resour. Res.* 47 (9): W09531. https://doi.org/10.1029/2011WR010591.

Legleiter, C. J., P. J. Kinzel, and B. T. Overstreet. 2011b. "Evaluating the potential for remote bathymetric mapping of a turbid, sand-bed river. 2: Application to hyperspectral image data from the Platte river: Remote bathymetric mapping, 2." *Water Resour. Res.* 47 (9): W09532. https://doi.org/10.1029/2011WR010592.

Legleiter, C. J., P. C. Kyriakidis, R. R. McDonald, and J. M. Nelson. 2011c. "Effects of uncertain topographic input data on two-dimensional flow modeling in a gravel-bed river: Effects of uncertain topographic input data." *Water Resour. Res.* 47 (3): W03518. https://doi.org/10.1029/2010WR009618.

Leopold, L. B., and M. G. Wolman. 1957. *River channel patterns: Braided, meandering and straight*, 85. Reston, VA: USGS.

Li, G. 2009. *Questions and answers about the Yellow river*. Zhengzhou, China: Yellow River Conservancy Press.

Liseĭkin, V. D. 2010. "Grid generation." In *Methods: Scientific computation*. Dordrecht, Netherlands: Springer.

Mangelsdorf, J., K. Scheurmann, and F.-H. Weiss. 1990. "River morphology: A guide for geoscientists and engineers." In *Springer series in physical environment*. New York: Springer.

McKean, J., D. Nagel, D. Tonina, P. Bailey, C. W. Wright, C. Bohn, and A. Nayegandhi. 2009. "Remote sensing of channels and riparian zones with a narrow-beam aquatic-terrestrial LIDAR." *Remote Sens.* 1 (4): 1065–1096. https://doi.org/10.3390/rs1041065.

McKean, J., D. Tonina, C. Bohn, and C. W. Wright. 2014. "Effects of bathymetric lidar errors on flow properties predicted with a multi-dimensional hydraulic model: Lidar bathymetry and hydraulic models." *J. Geophys. Res. Earth Surf.* 119 (3): 644–664. https://doi.org/10.1002/2013JF002897.

Merwade, V. 2009. "Effect of spatial trends on interpolation of river bathymetry." *J. Hydrol.* 371 (1–4): 169–181. https://doi.org/10.1016/j.jhydrol.2009.03.026.

Merwade, V., A. Cook, and J. Coonrod. 2008. "GIS techniques for creating river terrain models for hydrodynamic modeling and flood inundation mapping." *Environ. Modell. Software* 23 (10–11): 1300–1311. https://doi.org/10.1016/j.envsoft.2008.03.005.

Merwade, V. M., D. R. Maidment, and B. R. Hodges. 2005. "Geospatial representation of river channels." *J. Hydrol. Eng.* 10 (3): 243–251. https://doi.org/10.1061/(ASCE)1084-0699(2005)10:3(243).

Nittrouer, J. A., M. A. Allison, and R. Campanella. 2008. "Bedform transport rates for the lowermost Mississippi River." *J. Geophys. Res.* 113 (3): F03004. https://doi.org/10.1029/2007JF000795.

Pender, G., and S. Ne'elz. 2010. "Flood inundation modelling to support flood risk management." In *Flood risk science and management*, edited by G. Pender and H. Faulkner, 234–257. Oxford, UK: Wiley-Blackwell.

Qin, X., X. Fang, L. Chen, H. Zheng, J. Ma, and M. Zhang. 2019. "A line integral convolution method with dynamically determining step size and interpolation mode for vector field visualization." *IEEE Access* 7: 19414–19422. https://doi.org/10.1109/ACCESS.2019.2895857.

Roe, P. L. 1997. "Approximate riemann solvers, parameter vectors, and difference schemes." *J. Comput. Phys.* 135 (2): 250–258. https://doi.org/10.1006/jcph.1997.5705.

Schäppi, B., P. Perona, P. Schneider, and P. Burlando. 2010. "Integrating river cross section measurements with digital terrain models for improved flow modelling applications." *Comput. Geosci.* 36 (6): 707–716. https://doi.org/10.1016/j.cageo.2009.12.004.

Thanh, V. Q., D. Roelvink, M. van der Wegen, L. X. Tu, J. Reyns, and V. T. P. Linh. 2020. "Spatial topographic interpolation for meandering channels." *J. Waterway, Port, Coastal, Ocean Eng.* 146 (5): 04020024. https://doi.org/10.1061/(ASCE)WW.1943-5460.0000582.

Thompson, J. F., Z. U. A. Warsi, and C. W. Mastin. 1985. *Numerical grid generation: Foundations and applications*. New York: Elsevier.

Ueng, S. K., K. Sikorski, and Kwan-Liu. Ma. 1995. *Fast algorithms for visualizing fluid motion in steady flow on unstructured grids*. Contract No. NAS1-19480. Washington, DC: NASA Langley Research Center.

Valiani, A., and L. Begnudelli. 2006. "Divergence form for bed slope source term in shallow water equations." *J. Hydraul. Eng.* 132 (7): 652–665. https://doi.org/10.1061/(ASCE)0733-9429(2006)132:7(652).

Vanzo, D., A. Siviglia, and E. F. Toro. 2016. "Pollutant transport by shallow water equations on unstructured meshes: Hyperbolization of the model and numerical solution via a novel flux splitting scheme." *J. Comput. Phys.* 321 (Sep): 1–20. https://doi.org/10.1016/j.jcp.2016.05.023.

Vreugdenhil, C. B. 1994. "Numerical methods for shallow-water flow." In *Water science and technology library*. Boston: Kluwer Academic Publishers.

Wang, Z., J. Xia, M. Zhou, S. Deng, and T. Li. 2020. "Modelling hyperconcentrated floods in the Middle Yellow river using an improved river network model." *CATENA* 190 (Jul): 104544. https://doi.org/10.1016/j.catena.2020.104544.

Wheaton, J. M., J. Brasington, S. E. Darby, and D. A. Sear. 2009. "Accounting for uncertainty in DEMs from repeat topographic surveys: Improved sediment budgets." *Earth Surf. Processes Landforms* 35 (2): 136–156. https://doi.org/10.1002/esp.1886.

Williams, R. D., C. D. Rennie, J. Brasington, D. M. Hicks, and D. Vericat. 2015. "Linking the spatial distribution of bed load transport to morphological change during high-flow events in a shallow braided river: Spatially distributed bedload transport." *J. Geophys. Res. Earth Surf.* 120 (3): 604–622. https://doi.org/10.1002/2014JF003346.

Ye, X., D. Kao, and A. Pang. 2005. "Strategy for seeding 3D streamlines." In *Proc., VIS 05. IEEE Visualization, 2005*, 471–478. Minneapolis: IEEE. https://doi.org/10.1109/VISUAL.2005.1532831.

Zheng, S., B. Wu, C. R. Thorne, and G. Tan. 2015. "Case study of variation of sedimentation in the Yellow and Wei rivers." *J. Hydraul. Eng.* 141 (3): 05014009. https://doi.org/10.1061/(ASCE)HY.1943-7900.0000980.

Zhi, H., J. Siwabessy, S. L. Nichol, and B. P. Brooke. 2014. "Predictive mapping of seabed substrata using high-resolution multibeam sonar data: A case study from a shelf with complex geomorphology." *Mar. Geol.* 357 (Nov): 37–52. https://doi.org/10.1016/j.margeo.2014.07.012.